APPROXIMATING DISPERSIVE MATERIALS WITH PARAMETER DISTRIBUTIONS IN THE LORENTZ MODEL

JACQUELINE ALVAREZ AND ANDREW FISHER

ADVISOR: DR. NATHAN L. GIBSON
OREGON STATE UNIVERSITY

ABSTRACT. We seek to improve the accuracy of the Lorentz model by incorporating a distribution of parameters. Relevant background information is included along with a derivation of the Lorentz model. The forward problem in the frequency domain demonstrates the difference between the distributed and deterministic models. Using a least squares cost formulation and χ^2 significance test, we explore the inverse problem for saltwater data. In the forward problem of the time domain, Generalized Polynomial Chaos is applied to our random Lorentz model, eliminating dependence on the random variable. We discretize the model and Maxwell's equations using the Finite Difference Time Domain (FDTD) method according to the one dimensional Yee Scheme. Results are presented from the inverse problem using both single frequency sinewaves and ultra-wideband (UWB) pulses as interrogating signals. Lastly, we use the two dimension Yee Scheme to perform stability analysis for the random Lorentz model and our FDTD approximation.

1. INTRODUCTION

Electromagnetic interrogation of dispersive materials is of current interest in industry for its potential as a non-invasive method in identifying weaknesses or compositions in materials. An example is determining a material's dispersive properties through the analysis of a single transmitted ultra-wideband (UWB) pulse. Several different methods have been suggested that expand on the common Lorentz polarization model, some employing linear combinations of poles or normally distributed poles to fit data [4]. In this paper, however, we explore placing beta distributions on the dielectric parameters in the model.

First we present necessary background information including Maxwell's equations, the constitutive equations, and a derivation of the Lorentz model. Next we define random polarization and determine which parameters to distribute. Then using Fourier transforms, we explore the frequency domain through complex permittivity and present a couple inverse problems. For analysis in the time domain, we use Polynomial Chaos and the Finite Difference Time Domain (FDTD) method to discretize in one dimension according to the Yee Scheme. After examining two inverse time domain problems that compare interrogation signals, we finish by proving the stability of the random Lorentz model and its discretization.

Date: 8/18/2017.

This work was done during the 2017 REU program in mathematics at Oregon State University, with support by National Science Foundation Grant DMS-1359173.

2. BACKGROUND

2.1. **Maxwell's Equations.** We begin by presenting Maxwell's equations that describe the behavior of electromagnetic waves in free space. D and B are the electric and magnetic flux densities, E and H are the electric and magnetic fields, J is the conduction current density, and ρ is the charge density.

$$\frac{\partial D}{\partial t} + J = \nabla \times H \tag{1a}$$

$$\frac{\partial B}{\partial t} = -\nabla \times E \tag{1b}$$

$$\nabla \cdot D = \rho \tag{1c}$$

$$\nabla \cdot B = 0 \tag{1d}$$

Next, we incorporate the constitutive laws that adapt Maxwell's equations for propagation in materials. Additionally, $\tilde{\varepsilon}$ is electric permittivity and is equal to the product of the permittivity of free space and relative permittivity ($\tilde{\varepsilon} = \varepsilon_0 \varepsilon$). Magnetic permeability is given by μ, the material's polarization and conductivity are P and σ, and J_s is the source current.

$$D = \tilde{\varepsilon} E + P \tag{2a}$$

$$B = \mu H + M \tag{2b}$$

$$J = \sigma E + J_s \tag{2c}$$

To find the equations defining electromagnetic waves in a material, we substitute the constitutive equations into Maxwell's curl equations:

$$\tilde{\varepsilon}\frac{\partial E}{\partial t} = \nabla \times H - J - \frac{\partial P}{\partial t} = \nabla \times H - \sigma E - J_s - \frac{\partial P}{\partial t} \tag{3}$$

$$\mu \frac{\partial H}{\partial t} = -\nabla \times E - \frac{\partial M}{\partial t}. \tag{4}$$

Next, we restrict our discussion to the one dimensional case with waves propagating in the z-direction. Because electromagnetic waves are transverse with the electric and magnetic fields oscillating perpendicular to each other, we choose E and H to oscillate in the x and y directions, respectively. Prior to interrogation, there are no fields or polarizations present so our initial conditions are:

$$E(0,z) = H(0,z) = P(0,z) = 0. \tag{5}$$

Our boundary conditions include the interrogating signal, $f(t)$, at $z = 0$ and a reflective surface at $z = z_0$:

$$E(t,0) = f(t) \text{ and } E(t,z_0) = 0. \tag{6}$$

We also assume that our material is non-conducting with no magnetization or source current ($\sigma = 0$, $M = 0$, $\mu = \mu_0$ and $J_s = 0$):

$$\tilde{\varepsilon}\frac{\partial E_x}{\partial t} = -\frac{\partial H_y}{\partial z} - \frac{\partial P_x}{\partial t} \tag{7}$$

$$\mu_0\frac{\partial H_y}{\partial t} = -\frac{\partial E_x}{\partial z}. \tag{8}$$

where μ_0 is the magnetic permeability of free space. From now on, we drop the subscripts so that $E = E_x$, $P = P_x$, and $H = H_y$.

2.2. **Lorentz Model.** There are several models that describe polarization in materials. In this paper, we focus on the Lorentz model for which the physical assumption is that we can treat electrons in the material as simple harmonic oscillators (ie. electrons attached to little springs) [1]. We can then write down the second order differential equation for a damped, driven oscillator where ν is the damping coefficient, ω_0 is the natural resonant frequency, and x is the displacement:

$$m\ddot{x} + 2m\nu\dot{x} + m\omega_0^2 x = F_{driving}. \tag{9}$$

Recall that polarization can be defined as the electric dipole moment density and that the dipole moment between two equal charges is the product of their charge and displacement ($\vec{p} = q\vec{x}$). Then letting N be the electron density and $\vec{F_{driving}} = q\vec{E}$, we convert (9) into a differential equation relating the polarization and electric field:

$$\ddot{P} + 2\nu\dot{P} + \omega_0^2 P = \varepsilon_0\omega_p^2 E \quad \text{with} \quad \omega_p^2 = Nq^2/m\varepsilon_0. \tag{10}$$

It is helpful to note that ν and ω_p can be expressed in terms of a time constant τ and static permittivity ε_s where $\nu = \frac{1}{2\tau}$ and $\omega_p^2 = \omega_0^2(\varepsilon_s - \varepsilon_\infty)$ [2]. Using either Fourier or Laplace transforms, we can solve for the polarization as a convolution of the electric field:

$$P = \int_0^t g(t-s,x)E(s,x)dx \tag{11a}$$

$$g = \frac{\varepsilon_0\omega_p^2}{\nu_0}e^{-\nu t}\sin\nu_0 t \quad \text{and} \quad \nu_0 = \sqrt{\omega_0^2 - \nu^2}. \tag{11b}$$

The function g is the dielectric response function (DRF) and is responsible for how the polarization reacts to past electric fields. In other words, it encompasses the polarization's memory of the electric field. Plugging equation (10) into (2a) and taking the Fourier transform, we get $\hat{D} = \varepsilon_0\varepsilon(\omega)\hat{E}$ where $\varepsilon(\omega)$ is the complex permittivity given by

$$\varepsilon(\omega) = \varepsilon_\infty + \frac{\omega_p^2}{\omega_0^2 - \omega^2 + i2\nu\omega}. \tag{12}$$

For multiple poles, the permittivity merely includes a summation:

$$\varepsilon(\omega) = \varepsilon_\infty + \sum_{i=1}^{\infty}\frac{\omega_{p,i}^2}{\omega_{0,i}^2 - \omega^2 + i2\nu_i\omega}. \tag{13}$$

2.3. **Random Polarization.** In this paper, we research the effects of altering the original Lorentz model by applying a probability distribution to one of the parameters. In order to use distributions of parameters with Maxwell's equations, we define the random Lorentz model similar to (10) and (12), but where the distributed parameter is now a random variable and $\mathcal{P}$ is the random polarization:

$$\ddot{\mathcal{P}} + 2\nu\dot{\mathcal{P}} + \omega_0^2\mathcal{P} = \varepsilon_0\omega_p^2 E \tag{14}$$

$$\varepsilon(\omega) = \varepsilon_\infty + \frac{\omega_p^2}{\omega_0^2 - \omega^2 + i2\nu\omega}. \tag{15}$$

Next, we define the macroscopic polarization of (7) as the expected value of the random polarization where the undetermined parameter η is a random variable defined over [a,b] with probability density function $dF(\eta)$ [5]:

$$P(t,z) = \int_a^b \mathcal{P}(t,z;\eta)\, dF(\eta). \tag{16}$$

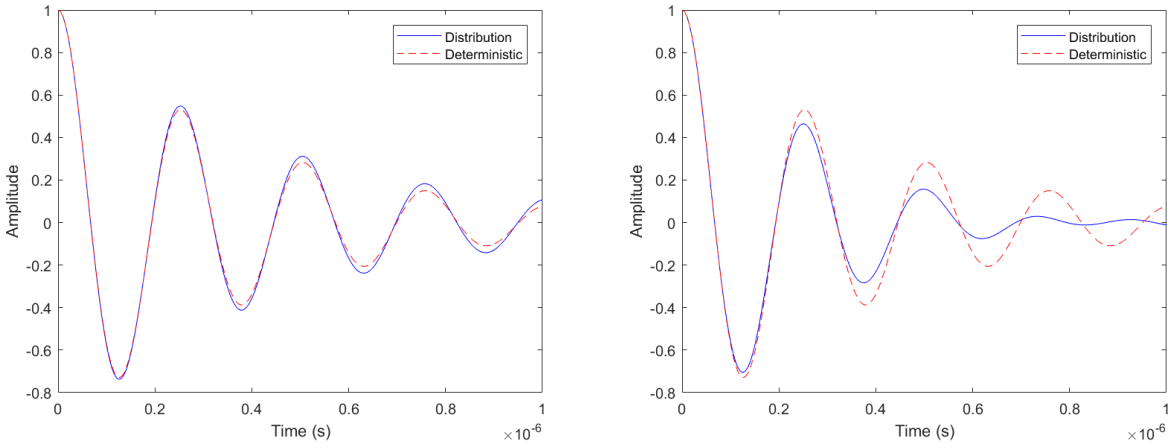

(A) ν Distribution: $\mathcal{U}(0.5\nu,1.5\nu)$ (B) ω_0^2 Distribution: $\mathcal{U}(0.75\omega_0^2,1.25\omega_0^2)$

FIGURE 1. Solutions for Unforced Differential Equation

First, we determine which parameters to vary: ν, ω_0, and/or ω_p. However, placing a distribution on ω_p doesn't change the form of the Lorentz model, it only scales the amplitude. To decide between ν and ω_0, we place a uniform distribution on each parameter and plot the solutions of the homogeneous differential equation using Monte Carlo sampling and common parameter values. The results are shown in Figure 1.

The distribution on ω_0 makes an appreciable difference in both amplitude and phase, while distributing ν hardly affects the solution. Thus, it would be more interesting and useful to distribute ω_0. But because ω_0 always appears as ω_0^2, we choose to vary ω_0^2 for simplicity.

3. Forward Simulation Frequency Domain

3.1. **Complex Permittivity and Index of Refraction.** Now we consider the frequency domain formulation of the random Lorentz model. First we break (12) into its real and imaginary parts, $\varepsilon = \varepsilon_r + i\varepsilon_i$:

$$\varepsilon_r = \varepsilon_\infty + \frac{\omega_p^2(\omega_0^2 - \omega^2)}{(\omega_0^2 - \omega^2)^2 + 4\nu^2\omega^2} \tag{17a}$$

$$\varepsilon_i = \frac{2\omega_p^2 \nu\omega}{\omega_p^2(\omega_0^2 - \omega^2)}. \tag{17b}$$

There is also a simple relationship between the complex permittivity and complex index of refraction [1]:

$$\tilde{n} = \sqrt{\frac{\varepsilon\varepsilon_0\mu}{\varepsilon_0\mu_0}} = \sqrt{\varepsilon} \tag{18}$$

where we hold the previous assumption that $\mu = \mu_0$.

The real part of $\tilde{n} = n + ik$ is the standard index of refraction that determines the speed of propagation, while the imaginary part is the extinction coefficient which determines the attenuation of a wave. Squaring both sides of (18) and equating real and imaginary parts, we arrive at a simple relation:

$$\varepsilon_r = n^2 - k^2 \tag{19a}$$

$$\varepsilon_i = 2kn. \tag{19b}$$

Experimental data is often measured in terms of index of refraction and attenuation, so these relations are useful in applying the Lorentz model.

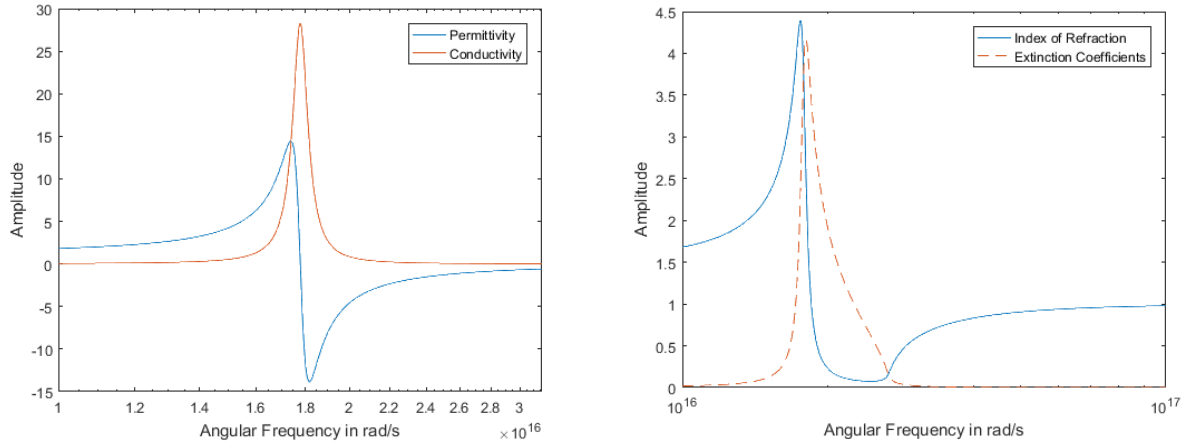

(A) Complex Permittivity (B) Complex Index of Refraction

Figure 2. Example Plots

3.2. **Analytic Integration.** Because ω_0^2 is a random variable, we must integrate over the probability distribution to find the expected permittivity. In the case of a uniform distribution over $[a,b]$, we can directly integrate (17a) and (17b) with respect to ω_0^2:

$$\frac{1}{b-a}\int_a^b \varepsilon_r d\omega_0^2 = \varepsilon_\infty + \frac{\omega_p^2}{2(b-a)}\left(\ln((\omega_0^2)^2 - 2\omega_0^2\omega^2 + \omega^4 + 4\nu^2\omega^2)\right)\Big|_a^b \tag{20a}$$

$$\frac{1}{b-a}\int_a^b \varepsilon_i d\omega_0^2 = \frac{\omega_p^2}{(b-a)}\arctan\left(\frac{\omega^2-\omega_0^2}{2\nu\omega}\right)\Big|_a^b. \tag{20b}$$

For the general case of using Jacobi polynomials with a beta distribution, one must resort to Monte Carlo sampling or numerical integration in order to compute the expected value.

Remark 3.1. *In this paper, we set the foundation for all Jacobi polynomials $P^{(\hat{\alpha},\hat{\beta})}$ and their corresponding beta distributions $\beta(\hat{\alpha}+1,\hat{\beta}+1)$. However, our simulations consider only the specific case of the Legendre polynomials with uniform distributions given by $\hat{\alpha}=\hat{\beta}=0$.*

4. Frequency Domain Inverse Problem

4.1. **Optimization.** The complex permittivity equations relate how a signal will propagate in a Lorentz material with given parameters. The frequency inverse problem involves recovering the parameters by fitting experimental data. Using a least squares cost formulation, we optimize using Matlab's lsqnonlin function. Letting the permittivity and conductivity be concatenated in a single vector V, the residue and cost are defined as:

$$R = V_{data} - V_{fit} \tag{21}$$

$$F = R^T R. \tag{22}$$

If the permittivity and conductivity are on the same order of magnitude, they don't need to be scaled.

We want to show whether distributed permittivities can be distinct from deterministic permittivites. For example, [10] discusses how the Lorenz-Lorentz model for permittivity is actually equivalent to the shifted Lorentz model with equivalence when the inequality $\frac{\omega p^2}{6\nu\omega_0} \ll 1$ is satisfied. To be sure the permittivites are distinct, we apply a deterministic fit to a distribution. For comparison, we plot the deterministic permittivity with the same parameters as the distribution. Results are shown in Figure 3 where the distribution's range is the radius over the midpoint (range $= \frac{b-a}{b+a}$).

Remark 4.1. *To avoid repeating units throughout the paper, we establish the units for the parameters in the Lorentz model: ω_0 and ω_p have units of rad/sec, τ has units of sec, and ν has units of 1/sec. Additionally, all frequencies are given in rad/sec.*

Table 1. Results for Saltwater Fits

Source	ε_∞	ν (1×10^{13})	ω_0 (1×10^{14})	Range	ω_p (1×10^{14})	Cost
Det. Fit	1.7931	2.7547	6.3568	–	1.7333	0.1704
Dist. Fit	1.7901	1.6112	6.3608	.0855	1.6067	0.0655

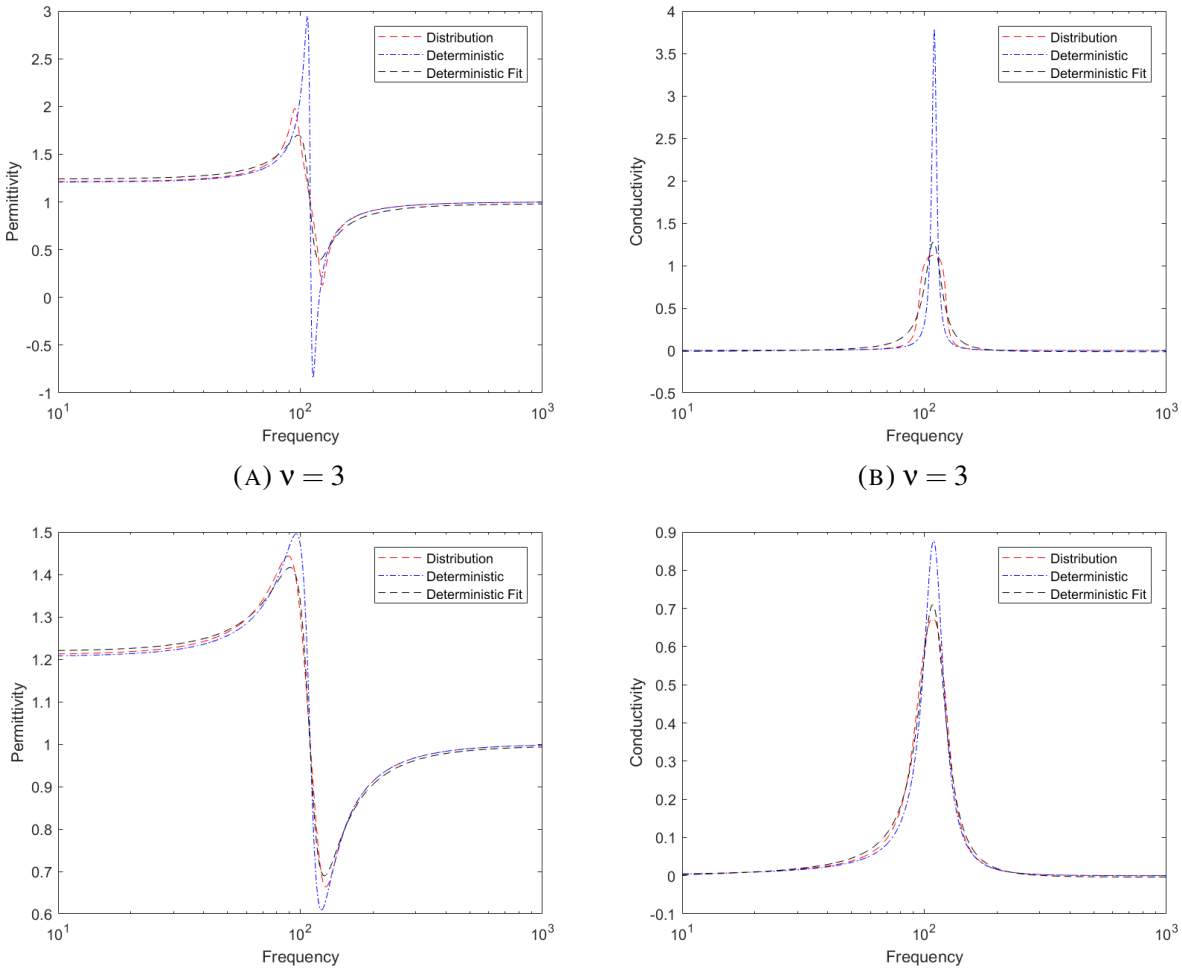

(A) $\nu = 3$ (B) $\nu = 3$

(C) $\nu = 13$ (D) $\nu = 13$

FIGURE 3. Parameters: $\omega_p = 50, \omega_0 = 110$, and range = .25

4.2. χ^2 **Testing.** As expected, the deterministic permittivity was unable to fit the distributed permittivity. To see how they compare, we fit actual saltwater data from [11]. The fits and results are shown in Figure 4 and Table 1.

To determine if there is statistical significance between the fits, we use the hypothesis testing presented in [3]. First we let $q = (\nu,\ \omega_0^2,\ \omega_p, \text{range}) \in Q$ where Q is the parameter set. Then, we define Q_0 to be the set $\{Q_0 \in Q : r = 0\}$ and let $\hat{q}_\ell$ and $\bar{q}_\ell$ denote minimizers of Q_0 and Q, respectively. We construct the hypotheses $H_0 : r = 0$ and $H_A : r \neq 0$ so that a rejection of the null hypothesis correlates to a difference in the fits. Finally, we define the test statistic:

$$U_\ell = \frac{\ell\,[F_\ell(\hat{q}_\ell) - F_\ell(\bar{q}_\ell)]}{F_\ell(\bar{q}_\ell)} \tag{23}$$

where ℓ is the number of data points and F_ℓ is the minimized cost.

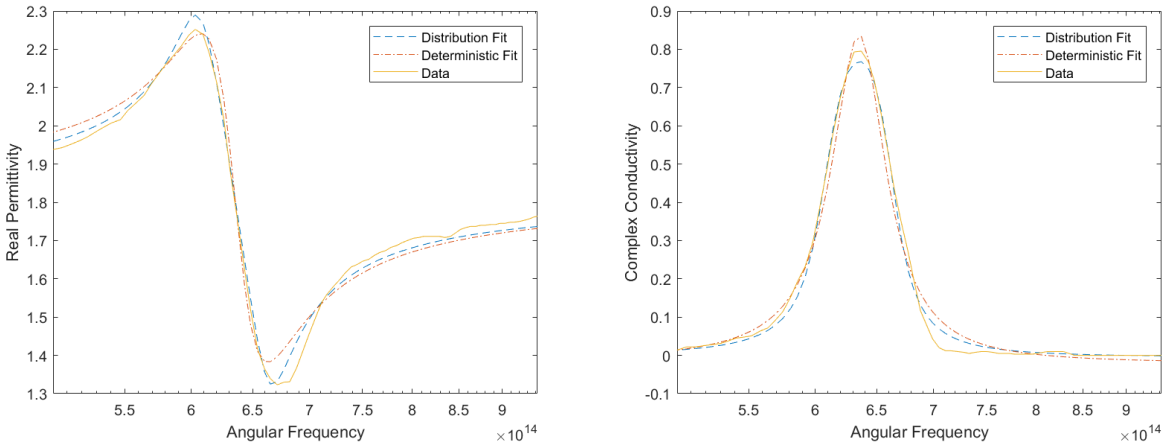

FIGURE 4. Fits for saltwater data

We proceed by using a significance level α and $\chi^2(s)$ distribution with s degrees of freedom to obtain the threshold τ so that $P\left(\chi^2(s) > \tau\right) = \alpha$. We compare U_ℓ with τ, such that if $U_\ell > \tau$ we reject the null hypothesis H_0. Because the parameter r is the only degree of freedom $(s = 1)$, we refer to Table 2.

TABLE 2. χ^2 distribution with 1 degree of freedom

$\alpha = .25$	$\tau = 1.32$
$\alpha = .10$	$\tau = 2.71$
$\alpha = .05$	$\tau = 3.84$
$\alpha = .01$	$\tau = 6.63$
$\alpha = .001$	$\tau = 10.83$

Our simulations return $F_\ell(\hat{q}) = 0.1704$ and $F_\ell(\bar{q}) = 0.0655$ with $\ell = 79$. Plugging those values into (23) we get $U_\ell = 126.584$. Because $U_\ell >> \tau$, we reject H_0. Thus, we can conclude that a distributed model provides a statistically significantly better fit than a deterministic model.

4.3. **Bimodal Data.** We also consider fitting bimodal data. First, we create data using a distribution with the parameters given in Table 3. Because real data requires repeated measurements, instrument errors can be propagated. For this reason, we add normally distributed noise with $\mu = 0$ and $\sigma = .001$ to the derivatives of the bimodal data. Then we optimize with uni-modal, bi-modal, and bi-discrete fits. Results are given in Table 3. As expected, the bi-modal fit best matches the data with $F = 0.1118$. We had hoped that the uni-modal and bi-discrete fits would be comparable, but the uni-modal cost was 10 times larger. We assumed that a single beta distribution with $\hat{\alpha}$ and $\hat{\beta}$ as parameters would give better results, but it only made slight improvements. The cost of the best fit was still 7 times larger than the bi-discrete fit.

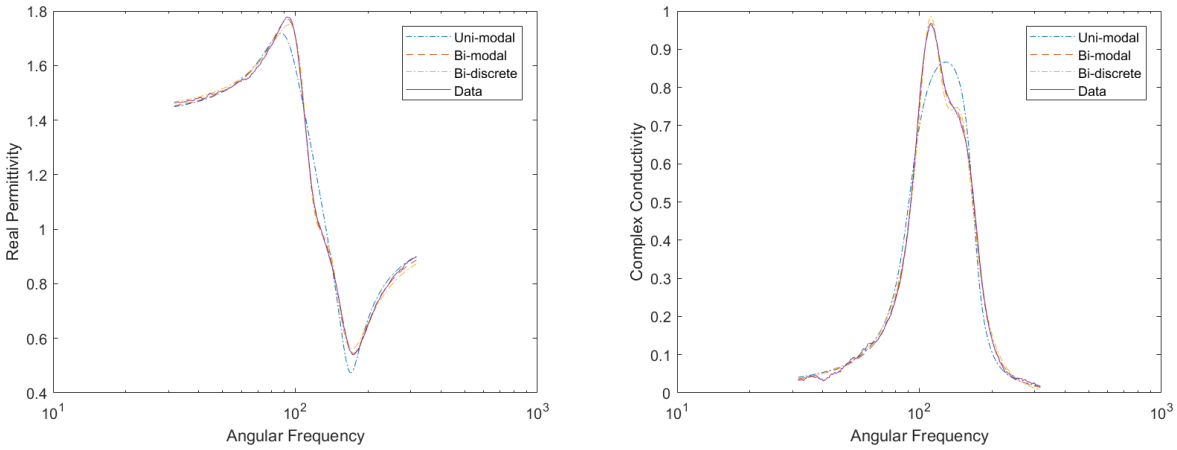

FIGURE 5. Fits for bimodal data

TABLE 3. Bimodal Fit Comparison

Source	ε_∞	ν	ω_0	Range	ω_p	ν_2	$\omega_{0,2}$	Range	$\omega_{p,2}$	Cost
Data	1.000	13.000	110.000	0.200	50.000	20.000	150.000	0.300	70.000	–
Uni-modal	0.986	14.659	134.811	0.539	83.861	–	–	–	–	4.763
Bi-modal	0.978	15.079	110.918	0.179	53.817	20.573	151.327	0.262	68.229	0.1118
Bi-discrete	0.970	17.693	111.580	–	55.571	27.731	151.144	–	71.073	0.4894

5. POLYNOMIAL CHAOS

5.1. **Polynomial Expansion.** Now we consider the time domain formulation of the random Lorentz model, using Polynomial Chaos to deal with the random variable ω_0^2. Polynomial Chaos is a method of solving random differential equations by expressing quantities as orthogonal polynomial expansions in the random variable [12]. We expand in the normalized Jacobi polynomials, but because they are defined on [-1,1] it is necessary to scale our distribution. Letting $\omega_0^2 = m + r\xi$ so that ξ is defined on [-1,1], we identify m and r as the center and radius of the distribution. Random polarization can now be expressed as a function of ξ,

$$\mathcal{P}(\xi,t) = \sum_{i=0}^{\infty} \alpha_i(t)\phi_i(\xi). \tag{24}$$

All orthogonal polynomials also satisfy the following recurrence relationship,

$$\xi\phi_n(\xi) = a_n\phi_{n+1}(\xi) + b_n\phi_n(\xi) + c_n\phi_{n-1}(\xi) \tag{25}$$

where the coefficients for the Jacobi polynomials are:

$$a_n = \frac{2(n+\hat{\alpha})(n+\hat{\beta})}{(2n+\hat{\alpha}+\hat{\beta})(2n+\hat{\alpha}+\hat{\beta}+1)}$$
$$b_n = \frac{\hat{\beta}^2-\hat{\alpha}^2}{(2n+\hat{\alpha}+\hat{\beta})(2n+\hat{\alpha}+\hat{\beta}+2)}$$
$$c_n = \frac{2(n+1)(n+\hat{\alpha}+\hat{\beta}+1)}{(2n+\hat{\alpha}+\hat{\beta}+1)(2n+\hat{\alpha}+\hat{\beta}+2)}.$$

Plugging (24) into (14) and replacing ω_0^2 with $m+r\xi$ gives,

$$\sum_{i=0}^{\infty} \ddot{\alpha}_i(t)\phi_i(\xi) + 2\nu\dot{\alpha}_i(t)\phi_i(\xi) + (r\xi+m)\alpha_i(t)\phi_i(\xi) = \varepsilon_0\omega_p^2 E\phi_0(\xi). \tag{26}$$

Then separating and using the recurrence relation (25), we have

$$\sum_{i=0}^{\infty} \left[\ddot{\alpha}_i(t) + 2\nu\dot{\alpha}_i(t) + m\alpha_i(t)\right]\phi_i(\xi) + r\sum_{i=0}^{\infty}\alpha_i(t)\left[a_i\phi_{i+1}(\xi) + b_i\phi_i(\xi) + c_i\phi_{i-1}(\xi)\right] = \varepsilon_0\omega_p^2 E\phi_0(\xi). \tag{27}$$

Taking the weighted inner product with respect to $\phi_j(\xi)$ for p orthogonal polynomials, we have

$$\sum_{i=0}^{p-1} \left[\ddot{\alpha}_i(t) + 2\nu\dot{\alpha}_i(t) + m\alpha_i(t)\right]\left\langle\phi_i,\phi_j\right\rangle + r\sum_{i=0}^{p-1}\alpha_i(t)\left[a_i\left\langle\phi_{i+1},\phi_j\right\rangle + b_i\left\langle\phi_i,\phi_j\right\rangle + c_i\left\langle\phi_{i-1},\phi_j\right\rangle\right] = \varepsilon_0\omega_p^2 E\phi_0(\xi) \tag{28}$$

where $\left\langle\phi_i,\phi_j\right\rangle$ for the normalized Jacobi polynomials is defined as:

$$\left\langle\phi_i,\phi_j\right\rangle := \int_{-1}^{1}\phi_i(\xi)\phi_j(\xi)w(\xi)d\xi = \begin{cases} 0 & \text{if } i\neq j \\ 1 & \text{if } i=j. \end{cases} \tag{29}$$

Because we've projected onto a finite number of basis polynomials, we can now express our system in matrix notation:

$$\vec{\ddot{\alpha}} + 2\nu\vec{\dot{\alpha}} + A\vec{\alpha} = \vec{f} \tag{30}$$

where $A = rM + mI$, $\hat{e}_1$ is the first standard column unit vector,

$$M = \begin{pmatrix} b_0 & c_1 & 0 & \cdots & 0 \\ a_0 & b_1 & c_2 & & \vdots \\ 0 & \ddots & \ddots & \ddots & 0 \\ \vdots & & a_{p-3} & b_{b-2} & c_{p-1} \\ 0 & \cdots & 0 & a_{p-2} & b_{p-1} \end{pmatrix} \text{ and } \vec{f} = \hat{e}_1\varepsilon_0\omega_p^2 E.$$

Letting $\dot{\vec{\alpha}} = \vec{\beta}$ we express (30) as a system of differential equations:

$$\dot{\vec{\alpha}} = \vec{\beta} \tag{31a}$$

$$\dot{\vec{\beta}} = -A\vec{\alpha} - 2\nu I\vec{\beta} + \vec{f}. \tag{31b}$$

5.2. **Eigenvalues.** It may also be convenient to combine (31) into a single first order matrix equation by letting $\vec{x} = \begin{pmatrix} \vec{\alpha} \\ \vec{\beta} \end{pmatrix}$:

$$\dot{\vec{x}} = B\vec{x} + \begin{pmatrix} \vec{0} \\ \vec{f} \end{pmatrix} \text{ where } B = \begin{pmatrix} \vec{0} & I \\ -A & -2\nu I \end{pmatrix} \tag{32}$$

where B is a $2p \times 2p$ matrix. We now show that you can find an expression for the $2p$ eigenvalues of B.

Let $\vec{v} = \begin{bmatrix} \vec{x}^T \vec{y}^T \end{bmatrix}^T$ be a nonzero eigenvector of $\bar{A}$, where $\vec{x}, \vec{y} \in \mathbb{C}^p$. Then for some $\lambda \in \lambda(B)$, we have

$$\begin{pmatrix} \vec{0} & I \\ -A & -2\nu I \end{pmatrix} \begin{pmatrix} \vec{x_1} \\ \vec{x_2} \end{pmatrix} = \lambda \begin{pmatrix} \vec{x_1} \\ \vec{x_2} \end{pmatrix}. \tag{33}$$

Next we separate the equations and eliminate $\vec{x_2}$:

$$\vec{x_2} = \lambda\vec{x_1}, \quad -A\vec{x_1} - 2\nu\vec{x_2} = \lambda\vec{x_2} \Rightarrow -A\vec{x_1} - 2\nu\lambda\vec{x_1} = \lambda^2\vec{x_1}. \tag{34}$$

Now replace A with $rM + mI$ and solve for $M\vec{x_1}$:

$$M\vec{x_1} = \frac{\lambda^2 + 2\nu\lambda + m}{-r}\vec{x_1}. \tag{35}$$

This is exactly the eigenvalue equation for the recursion matrix M, so $\frac{\lambda^2+2\nu\lambda+m}{-r} \in \lambda(M)$. It is known that the eigenvalues of any Jacobi recursion matrix are exactly the roots of the corresponding p^{th} order Jacobi polynomial [9]. Letting x_r denote the p roots, we have:

$$\frac{\lambda^2 + 2\nu\lambda + m}{-r} = x_r. \tag{36}$$

Solving the quadratic for each of the p roots gives the $2p$ eigenvalues of the B matrix:

$$\lambda = -\nu \pm \sqrt{\nu^2 - (m + rx_r)}. \tag{37}$$

In Figure 6 we plot the real and positive imaginary parts of all $\lambda \in \lambda(B)$ for a uniform distribution with test values of $\nu = 2.5 \times 10^6$, $\omega_0 = 2.5 \times 10^7$, $m = \omega_0^2$, and $r = .25\omega_0^2$. Notice that the negative imaginary parts are just complex conjugates. Also, realize that the real part is $-\nu$ for any p and that the complex part is bound above and below as p increases. Because $x_r \in [-1, 1]$, our result predicts bounds of $i\sqrt{m - r - \nu^2}$ and $i\sqrt{m + r - \nu^2}$ or $imag(\lambda) \in [2.15 \times 10^7, 2.79 \times 10^7]$ which agree with Figure 6.

We assumed complex eigenvalues for the previous analysis. If the eigenvalues were real, we would have a two pole Debye model defined by a first order differential equation. For this reason, the parameters must satisfy $r < m - \nu^2$, providing a bound on the distribution radius.

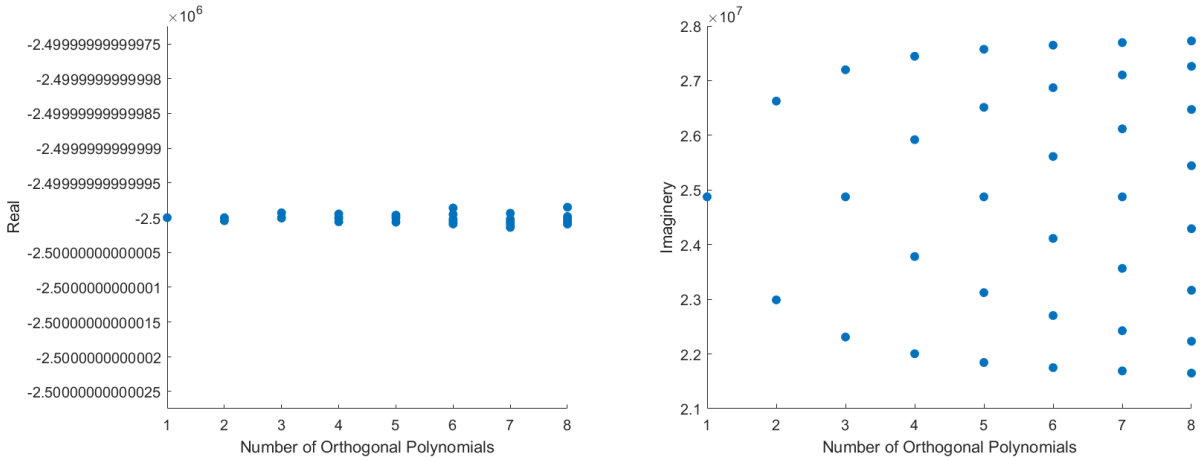

FIGURE 6. Scatter Plot of Eigenvalues

6. FORWARD SIMULATION TIME DOMAIN

6.1. **FDTD Discretization.** Combining Maxwell's equations with our results from Polynomial Chaos, we have the four equations that completely determine propagation through a dielectric material. We repeat them here as a reference:

$$\varepsilon_\infty \varepsilon_0 \frac{\partial E}{\partial t} = -\frac{\partial H}{\partial z} - \beta_0 \tag{38a}$$

$$\frac{\partial H}{\partial t} = -\frac{1}{\mu_0}\frac{\partial E}{\partial z} \tag{38b}$$

$$\dot{\vec{\alpha}} = \vec{\beta} \tag{38c}$$

$$\dot{\vec{\beta}} = -A\vec{\alpha} - 2\nu I\vec{\beta} + \vec{f}. \tag{38d}$$

It is important to note that $\frac{\partial P}{\partial t}$ is the time change in macroscopic polarization or the time change of the expected value of our random polarization. Since only the 0^{th} Jacobi polynomial is constant, we identify $\beta_0 = \frac{\partial P}{\partial t}$ with the other polynomials and coefficients determining uncertainties. This explains our substitution in (38a).

To model these equations, we discretize them according to the one-dimensional Yee Scheme [13]. The Yee Scheme implements a staggered grid where the electric field and random polarization are evaluated at integer time steps and spatial steps, while the magnetic field is evaluated at half integer time steps and spatial steps. We consider the domain $z \in [0, z_0]$ for $t \in [0, T]$, choosing integers J and N to discretize so that $\Delta z = \frac{z_0}{J}$ and $\Delta t = \frac{T}{N}$. Let $z_j = j\Delta z$ and $t^n = n\Delta t$. If U is a field variable, we define the grid function to be

$$U_j^n \approx U(x_j, t^n).$$

Our discrete initial conditions and boundary conditions are:

$$E_j^0 = \vec{\alpha}_j^0 = \vec{\beta}_j^0 = 0 \text{ for } 0 \le j \le J, \quad H_j^n = 0 \text{ for } 0 \le j \le J \text{ and } n \le 0,$$

$$E_0^n = f(t^n) \text{ and } E_J^n = 0 \text{ for } 0 \le n \le N.$$

First we approximate derivatives with finite differences and constant terms with averages:

$$\varepsilon_\infty \varepsilon_0 \frac{E_j^{n+1} - E_j^n}{\Delta t} = -\frac{H_{j+\frac{1}{2}}^{n+\frac{1}{2}} - H_{j-\frac{1}{2}}^{n+\frac{1}{2}}}{\Delta z} - \frac{\beta_{0,j}^{n+1} + \beta_{0,j}^n}{2} \tag{39a}$$

$$\frac{H_{j+\frac{1}{2}}^{n+\frac{1}{2}} - H_{j+\frac{1}{2}}^{n-\frac{1}{2}}}{\Delta t} = -\frac{1}{\mu_0} \frac{E_{j+1}^n - E_j^n}{\Delta z} \tag{39b}$$

$$\frac{\vec{\alpha}_j^{n+1} - \vec{\alpha}_j^n}{\Delta t} = \frac{\vec{\beta}_j^{n+1} + \vec{\beta}_j^n}{2} \tag{39c}$$

$$\frac{\vec{\beta}_j^{n+1} - \vec{\beta}_j^n}{\Delta t} = -A \frac{\vec{\alpha}_j^{n+1} + \vec{\alpha}_j^n}{2} - 2\nu I \frac{\vec{\beta}_j^{n+1} + \vec{\beta}_j^n}{2} + \frac{\hat{e}_1 \varepsilon_0 \omega_p^2}{2} \left[E_j^{n+1} + E_j^n \right]. \tag{39d}$$

Equations (39a), (39c), and (39d) are defined for $\{1 \le j \le J-1,\ 0 \le n \le N-1\}$ and (39b) is defined for $\{0 \le j \le J-1,\ 0 \le n \le N-1\}$.

Because $\vec{\alpha}, \vec{\beta}$, and E are defined at the same time steps, we have a coupled system of equations. Solving (39a)-(39c) for the next time step, we get

$$E_j^{n+1} = E_j^n + \frac{\Delta t}{\varepsilon_\infty \varepsilon_0 \Delta z} \left[H_{j+\frac{1}{2}}^{n+\frac{1}{2}} - H_{j-\frac{1}{2}}^{n+\frac{1}{2}} \right] - \frac{\Delta t \hat{e}_1^T}{2\varepsilon_\infty \varepsilon_0} \left[\vec{\beta}_j^{n+1} + \vec{\beta}_j^n \right] \tag{40a}$$

$$H_{j+\frac{1}{2}}^{n+\frac{1}{2}} = H_{j+\frac{1}{2}}^{n-\frac{1}{2}} + \frac{\Delta z}{\mu_0 \Delta z} \left[E_{j+1}^n - E_j^n \right] \tag{40b}$$

$$\vec{\alpha}_j^{n+1} = \vec{\alpha}_j^n + \frac{\Delta t}{2} \left[\vec{\beta}_j^{n+1} + \vec{\beta}_j^n \right]. \tag{40c}$$

Now, we insert (40a) into (39d) and multiply by $2\Delta t$:

$$\begin{aligned} 2\vec{\beta}_j^{n+1} - 2\vec{\beta}_j^n = &-\Delta t A \left[\vec{\alpha}_j^{n+1} + \vec{\alpha}_j^n \right] - 2\nu I \Delta t \left[\vec{\beta}_j^{n+1} + \vec{\beta}_j^n \right] \\ &+ \hat{e}_1 \varepsilon_0 \omega_p^2 \Delta t \left(2E_j^n + \frac{\Delta t}{\varepsilon_0 \varepsilon_\infty \Delta z} \left[H_{j+\frac{1}{2}}^{n+\frac{1}{2}} - H_{j-\frac{1}{2}}^{n+\frac{1}{2}} \right] - \frac{\Delta t \hat{e}_1^T}{2\varepsilon_0 \varepsilon_\infty} \left[\vec{\beta}_j^{n+1} + \vec{\beta}_j^n \right] \right). \end{aligned} \tag{41}$$

Then inserting (40c) into (41), we can simplify and collect terms such that

$$\left[2I + \frac{\Delta t^2 A}{2} + 2\nu \Delta t I + C \right] \vec{\beta}_j^{n+1} = \left[2I - \left(\frac{\Delta t^2 A}{2} + 2\nu \Delta t I + C \right) \right] \vec{\beta}_j^n - 2\Delta t A \vec{\alpha}_j^n + \hat{e}_1 G \tag{42}$$

with $C = \begin{pmatrix} \frac{\omega_p^2 \Delta t^2}{2\varepsilon_\infty} & 0 & 0 \\ 0 & 0 & 0 \\ 0 & 0 & 0 \end{pmatrix}$ and $G = 2\varepsilon_0 \omega_p^2 \Delta t E_j^n + \frac{\omega_p^2 \Delta t^2}{\varepsilon_\infty \Delta z} \left[H_{j+\frac{1}{2}}^{n+\frac{1}{2}} - H_{j-\frac{1}{2}}^{n+\frac{1}{2}} \right]$.

Then let

$$\bar{A} = \frac{\Delta t^2}{2} A + 2\nu \Delta t I + C \tag{43}$$

such that

$$\left(2I + \bar{A}\right) \vec{\beta}_j^{n+1} = \left(2I - \bar{A}\right) \vec{\beta}_j^{n} - 2\Delta t A \vec{\alpha}_j^{n} + \hat{e}_1 G. \tag{44}$$

Inverting $2I + \bar{A}$ allows us to solve for $\vec{\beta}^{n+1}$. Then using back substitution with (40c) and (40a), we can solve for $\vec{\alpha}^{n+1}$ and E^{n+1}.

6.2. **Invertibility of $2I + \bar{A}$.** To solve (44) for $\vec{\beta}^{n+1}$, we must show that $2I + \bar{A}$ is always invertible.

Theorem 6.1. *For the Jacobi polynomials, $2I + \bar{A}$ is invertible if $m > r$.*

Proof. First, we recall that a diagonally dominant matrix is invertible where diagonally dominant matrices satisfy

$$|a_{ii}| > \sum_{j \neq i} |a_{ij}| \ for\ all\ i. \tag{45}$$

It was shown in [6] that the recurrence matrix M is diagonally dominant as long as $m > r$, which is a physical restriction since all parameters must be positive. It is also clear that every other term of $2I + \bar{A}$ is diagonally dominant as well, since all terms are positive and appear on diagonals. Therefore, $2I + \bar{A}$ is invertible if $m > r$. □

6.3. **Simulation Convergence.** We now show that the Polynomial Chaos method converges quickly in p. We assume the material parameters $\tau = 7 \times 10^{-16}$, $\omega_0 = 1.8 \times 10^{16}$, and $\omega_p = 2 \times 10^{16}$ from [2]. Choosing the interrogating signal as a sine wave with angular frequency of 6×10^{15} and duration of 5 periods, we plot the signals at $t = 1.4 \times 10^{-5}$ ns for four different p values in Figure 7.

The signals for $p = 3$ and $p = 4$ are indistinguishable on the plots. The approximate relative errors of $p = 2$ and $p = 3$ compared to $p = 4$ are .56% and 0.014%, respectively. Thus, an expansion of three polynomials accurately approximates the convergence for large p. However, due to the high resonant frequencies of Lorentz materials, time steps and simulations must be very short. Therefore, small discrepancies might lead to more significant errors on a larger simulation.

7. Time Domain Inverse Problem

7.1. **Parameters.** In this section, we apply our forward simulation to the time domain inverse problem. It was proven in [5] that unique solutions exist for inverse problems posed with distributions over parameters. Specifically, we wish to reconstruct the parameters of a material from noisy data collected by a receiver a distance of .252 μm into the material. We borrow parameter values from [2]. Assuming $\varepsilon_0 = 1$ and that the interrogating signal is known, only three parameters need to optimized: τ, ω_0, and ω_p. Recall that τ and ν are related by the expression $\tau = \frac{1}{2\nu}$; we use tau for simulation purposes.

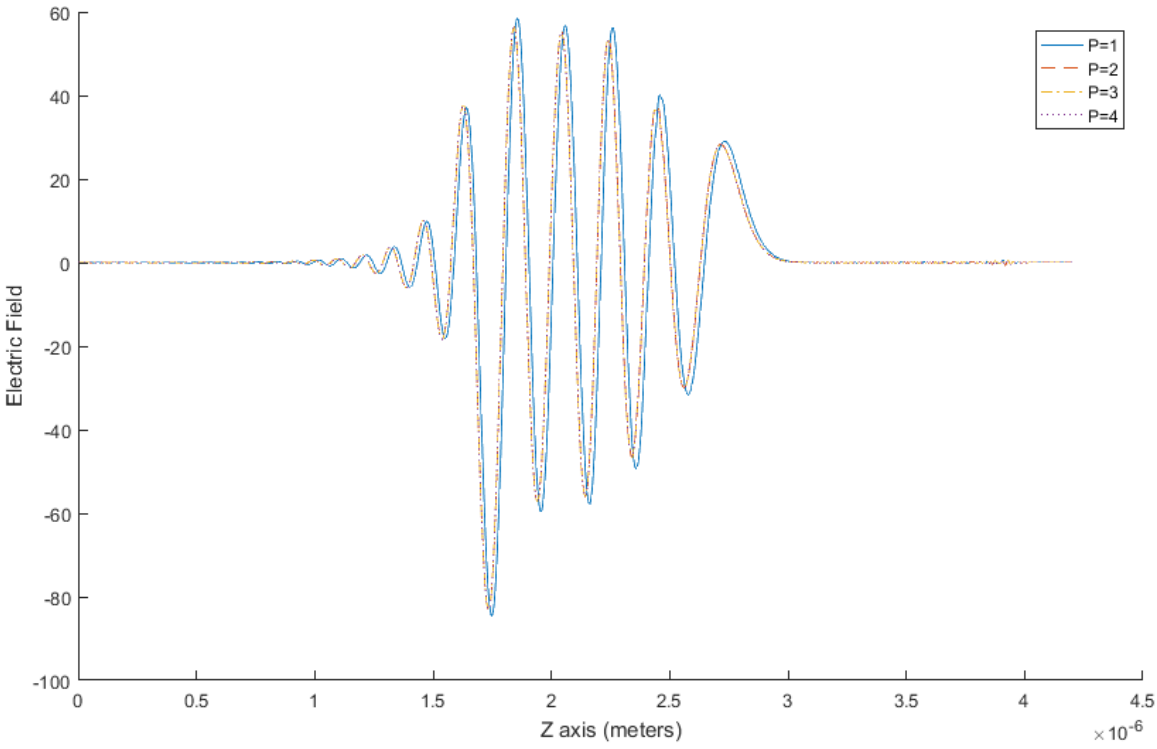

(A)

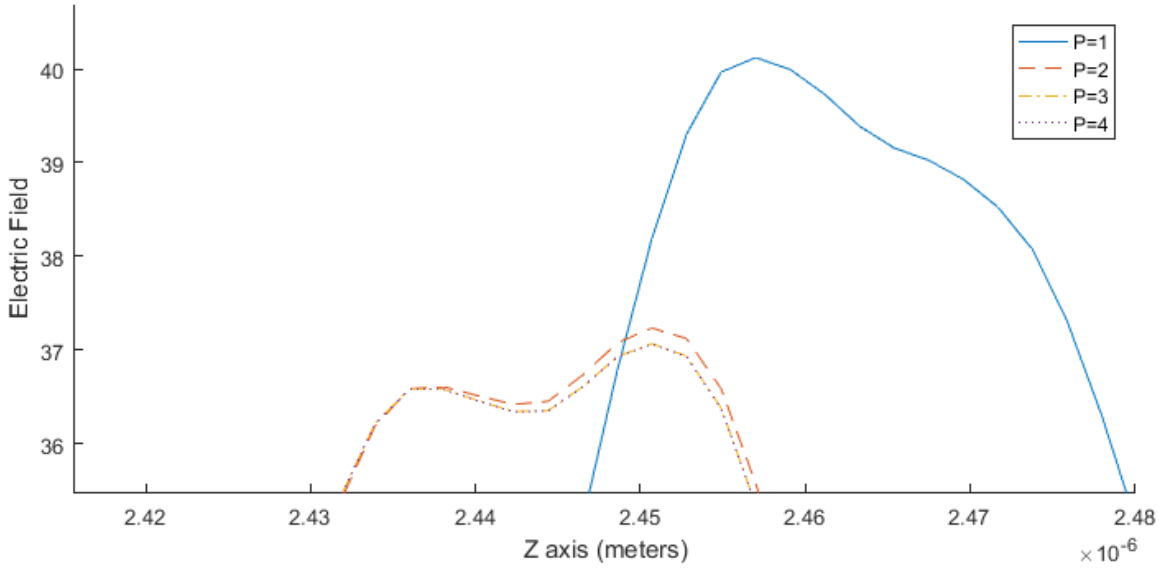

(B)

FIGURE 7. P-Convergence of Forward Simulation at $t = 1.4 \times 10^{-5}$ ns.

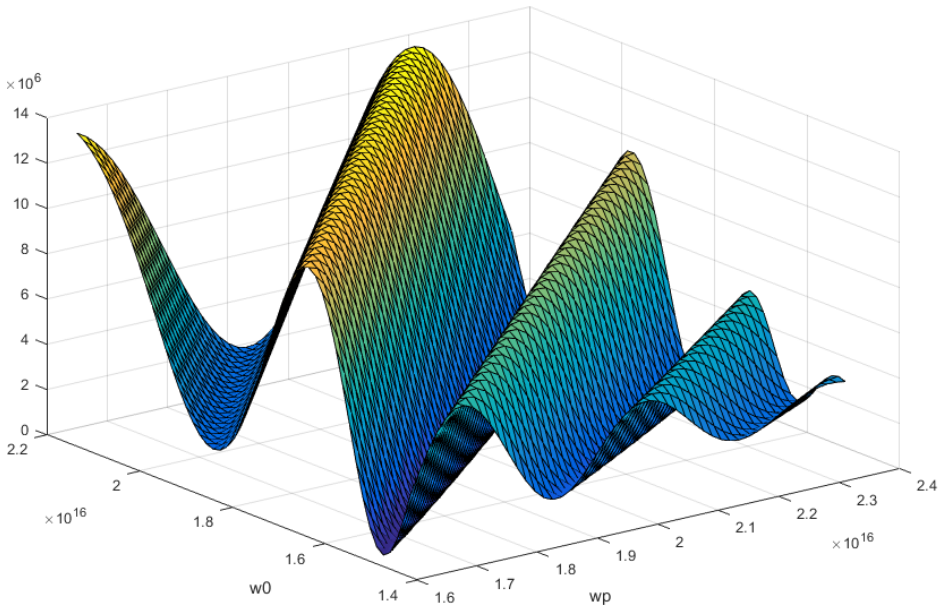

(A) Cost Function for Constant τ

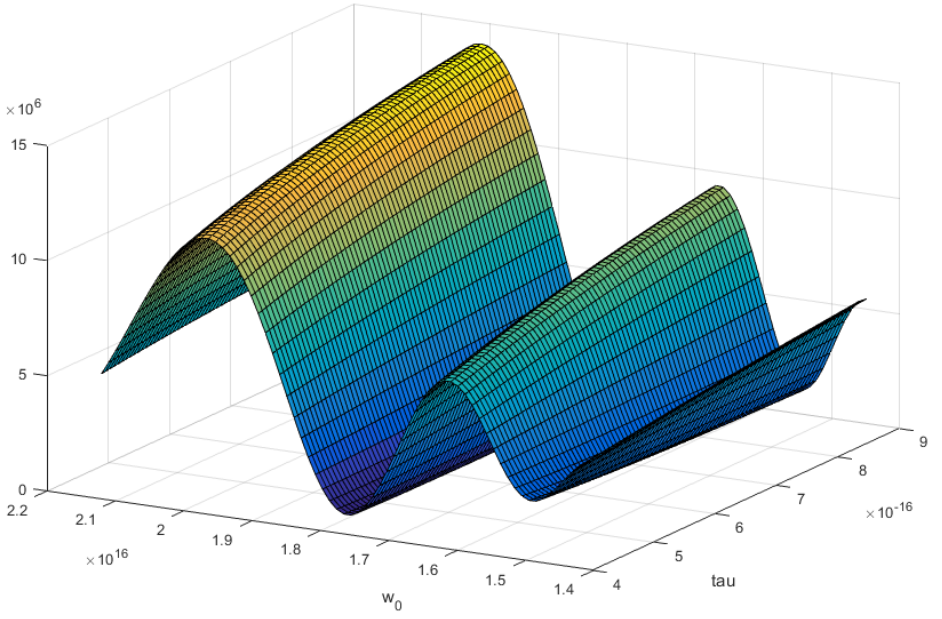

(B) Cost Function for Constant ω_p

FIGURE 8

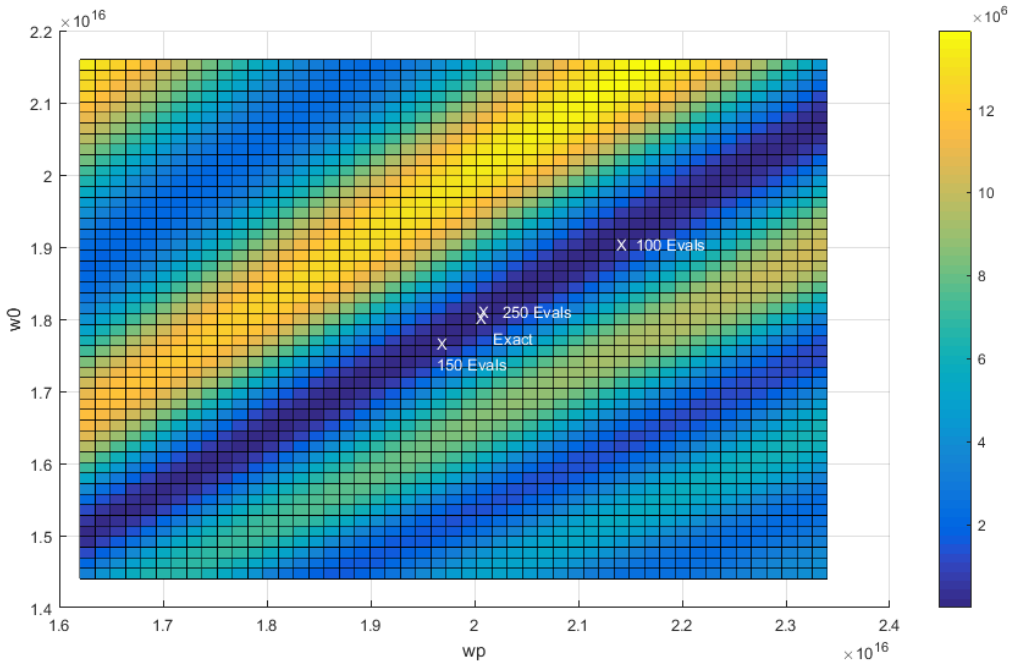

FIGURE 9. Convergence of Direct Algorithm

7.2. **Optimization.** Letting the column vector V denote the received signal, we define the cost and residue (F and R) as in (21) and (22). To understand the cost function's dependence on parameters, we made two surface plots in Figures 8a and 8b, fixing a different parameter in each. Notice that changes in τ don't affect the cost function nearly as much as changes in ω_0 or ω_p. This behavior determines our optimization strategy.

We use both Finkel's Direct program [8] and Matlab's lsqnonlin function. Direct takes the n-dimensional rectangular region determined by given bounds and iteratively divides into smaller rectangles, checking for possible minimums. In this way, Direct is able to find the global minimum for functions with several local minima. On the other hand, Matlab's lsqnonlin function uses gradient methods to converge quickly to the nearest local minimum.

Our strategy is to obtain an approximate solution using Direct to optimize ω_0 and ω_p, and then finish optimizing all three parameters with lsqnonlin. We justify this approach by fitting deterministic data with a deterministic fit so that an exact solution exists. We set the bounds as $\tau \in [4.44\times10^{-16}, 8.89\times10^{-16}]$, $\omega_0 \in [1.26\times10^{16}, 2.16\times10^{16}]$, and $\omega_p \in [1.62\times10^{16}, 2.52\times10^{16}]$.

In Figure 9, we plot the true minimum along with the minimums found by Direct for a given number of function evaluations. Here τ is fixed at the correct value, so Direct only optimizes ω_0 and ω_p. It had no problem finding the right valley, but took many evaluations to converge; $F = 132$ after 250 evaluations. Next, we tested our method running Direct for 100 evaluations before using lsqnonlin. We quickly found the solution of $\tau = 7\times10^{-16}, \omega_0 = 1.8\times10^{16}$, and $\omega_p = 2\times10^{16}$ with $F = 3\times10^{-20}$. We also tried optimizing all three parameters using Direct, but $F = 1,800,000$ after 300 evaluations.

For the first inverse problem, we consider how the deterministic model fits a distribution for single frequency signals. Data is created from a distribution with a range of 0.25 and normally-distributed noise. We run simulations where noise had mean 0 with standard deviations of 0, 1, and 2. Because some frequencies require longer measurements, we include normalized cost defined as the average cost per data point. Note that on average, adding noise with a standard deviation of σ increases the normalized cost by σ^2. Results are given in Table 4.

TABLE 4. Simulation Results for Single Frequency Signals

Noise Dev.	Ang. Freq.	τ (1×10^{-16})	ω_0 (1×10^{16})	ω_p (1×10^{16})	Cost	Norm. Cost
0	8e15	6.9537	1.7532	1.9683	513	0.085
0	1e16	6.8925	1.7500	1.9640	1174	0.196
0	3e16	6.7148	1.7861	2.0140	585	0.146
1	8e15	6.9402	1.7537	1.9687	6416	1.069
1	1e16	6.9066	1.7501	1.9640	7311	1.218
1	3e16	6.7061	1.7867	2.0133	4515	1.129
2	8e15	6.9778	1.7503	1.9642	23269	3.878
2	1e16	6.9498	1.7473	1.9595	25429	4.238
2	3e16	6.6906	1.7854	2.0142	16141	4.035

The deterministic model fits the data fairly well, but the optimized parameters change for different fits. One can also see that τ varied more for different amounts of noise than ω_0 and ω_p. This suggests that the inverse problem would provide more accurate estimations of ω_0 and ω_p than τ. In Figure 10a, we apply both deterministic and distributed fits for the 8×10^{15} frequency signal with noise of $\sigma = 2$ for comparison. Results are given in Table 5. Even though our method accurately recovered the true values of the material, the distributed fit was unable to significantly improve on the deterministic fit.

TABLE 5. Fit Comparison: Freq$= 8\times10^{15}$ and $\sigma = 2$

Source	τ (1×10^{-16})	ω_0 (1×10^{16})	Range	ω_p (1×10^{16})	Cost	Norm. Cost
Data	7	1.8	.25	2	–	–
Det. Fit	6.9489	1.7543	–	1.9697	23971	3.995
Dist. Fit	6.9819	1.8049	.2438	1.9984	23591	3.932
Dist. Error	-0.26%	0.27%	-2.48%	-0.08%	–	–

For the second inverse problem, we create data from the same distribution and attempt to apply deterministic and distributed fits. However, we now use a UWB as our interrogating signal:

$$f(t) = \sum_{i=1}^{n} \alpha_i \sin(f_i t) \tag{46}$$

where f_i is a vector of angular frequencies linearly spaced from 1×10^{14} to 1×10^{16} and α_i are weights determined by the beta distribution $\beta(1,3)$. Figure 10b shows the deterministic and distributed fits for noise with $\sigma = 2$. Results are given in Table 6. It is clearly harder for the deterministic model to fit a UWB than a single frequency signal.

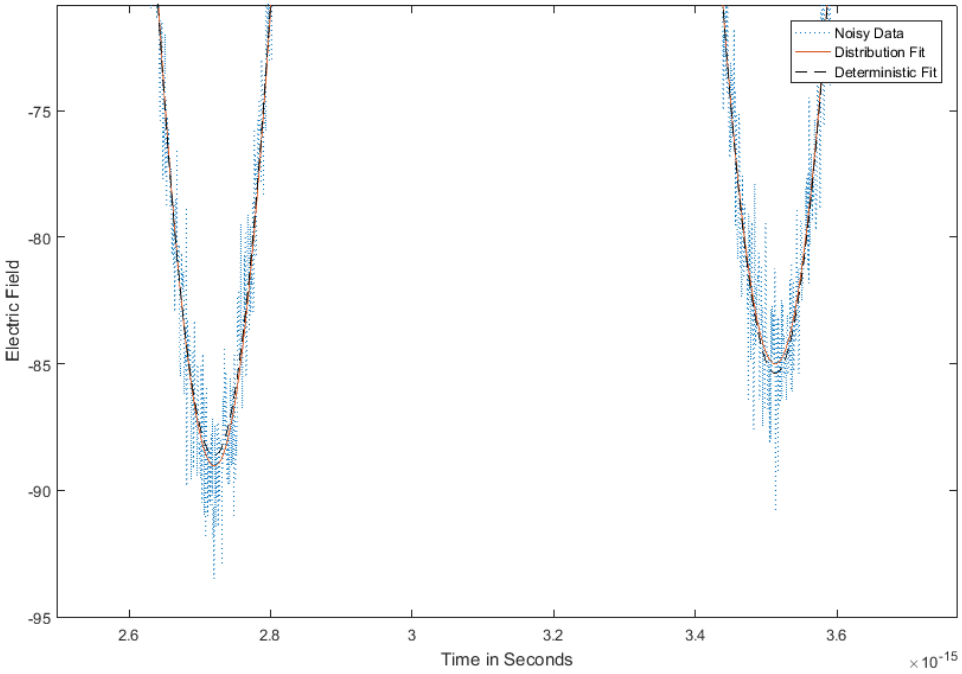

(A) Single Frequency Fits, $\sigma = 2$

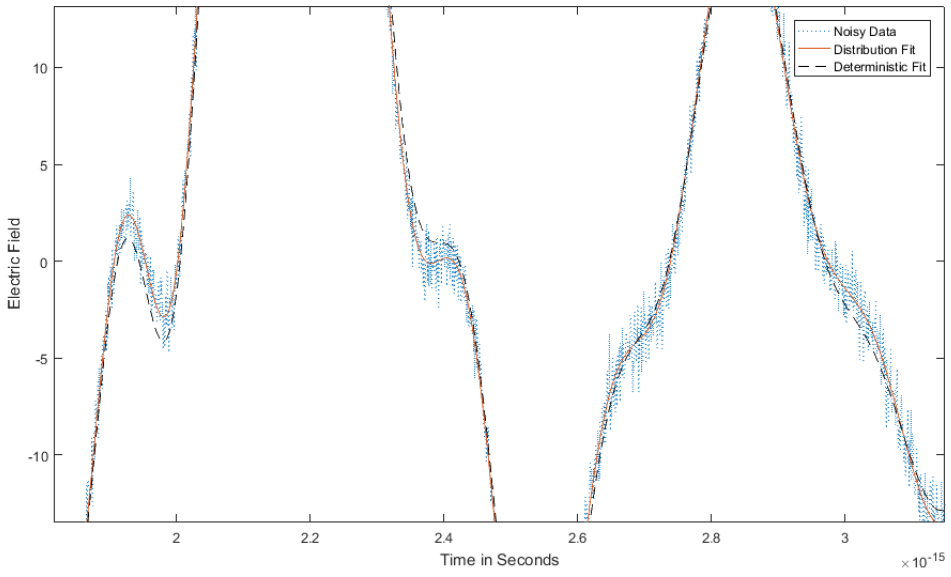

(B) UWB Fits, $\sigma = 2$

FIGURE 10. Close Comparison of Fits

TABLE 6. Fit Comparison: UWB with $\sigma = 2$

Source	τ (1×10^{-16})	ω_0 (1×10^{16})	Range	ω_p (1×10^{16})	Cost	Norm. Cost
Data	7	1.8	.25	2	–	–
Det. Fit	6.4433	1.7757	–	2.0135	25825	4.304
Dist. Fit	7.0650	1.7999	0.2493	1.9998	23441	3.907
Dist. Error	0.93%	-0.006%	-.28%	-0.01%	–	–

The data supports the suggestion above that the distributed model struggles with estimating τ from the data. This is expected since a large change in τ corresponds to a small change in the cost function. Also, the distributed fit did make an appreciable difference over the cost of the deterministic fit. This agrees with our simulations in the frequency domain where the deterministic model was unable to fit the distributed permittivity over a spectrum of frequencies.

8. STABILITY

8.1. **2D Random Lorentz Model.** Here we show the stability of the random Lorentz model in a two dimensional domain $\mathcal{D}$, similar to the work for the random Debye model in [7]. However, the analysis could easily be generalized to three dimensions. First, we give Maxwell's Equations for two dimensions along with the random Lorentz differential equation written as a system of first order equations. To do this, we define the scalar curl operator on a vector field $\mathbf{U} = (U_x, U_y)^T$ as $\text{curl}\,\mathbf{U} = \frac{\partial U_y}{\partial x} - \frac{\partial U_x}{\partial y}$, and the vector curl operator on the scalar field V to be $\mathbf{curl}\,V = \left(\frac{\partial V}{\partial y}, -\frac{\partial V}{\partial x}\right)^T$.

$$\mu_0 \frac{\partial H}{\partial t} = -\,\text{curl}\,\mathbf{E} \tag{47a}$$

$$\varepsilon_0 \varepsilon_\infty \frac{\partial \mathbf{E}}{\partial t} = \mathbf{curl}\,H - \mathbf{J} \tag{47b}$$

$$\frac{\partial \mathcal{P}}{\partial t} = \mathcal{J} \tag{47c}$$

$$\frac{\partial \mathcal{J}}{\partial t} = -2\nu\mathcal{J} - \omega_0^2 \mathcal{P} + \varepsilon_0 \omega_p^2 \mathbf{E} \tag{47d}$$

Next we define the vector spaces,

$$H(\text{curl}, \mathcal{D}) = \{\mathbf{u} \in \left(L^2(\mathcal{D})\right)^2; \text{curl}\,\mathbf{u} \in L^2(\mathcal{D})\} \tag{48}$$

$$H_0(\text{curl}, \mathcal{D}) = \{\mathbf{u} \in H(\text{curl}, \mathcal{D}), \mathbf{n} \times \mathbf{u} = 0\} \tag{49}$$

where $(\cdot,\cdot)_2$ and $||\cdot||_2$ denote the L^2 inner product and norm. Realize that the boundary restriction of H_0 for an electric field is equivalent to a perfect conducting (PEC) boundary condition. This PEC condition is necessary so that Green's formula for the **curl** operator holds.

$$(\mathbf{curl}\,H, \mathbf{u}) = (H, \text{curl}\,\mathbf{u}), \ \forall \mathbf{u} \in H_0(\text{curl}, \mathcal{D}) \tag{50}$$

We also introduce the Hilbert space $V_F = (L^2(\Omega))^2 \otimes (L^2(\mathcal{D}))^2$ where Ω is the distribution [a,b] on ω_0^2. The inner product and norm are defined as follows:

$$(u,v)_F = \mathbb{E}[(u,v)_2]$$
$$\|u\|_F^2 = \mathbb{E}[\|u\|_2^2].$$

Multiplying (47a) by $v \in L^2(\mathcal{D})$, (47b) by $\mathbf{u} \in H_0(\text{curl},\mathcal{D})$, (47c) and (47d) by $\mathbf{w_1}, \mathbf{w_2} \in \left(L^2(\mathcal{D})\right)^2$, and integrating over the domain $\mathcal{D}$, we arrive at the weak formulation:

$$\left(\mu_0 \frac{\partial H}{\partial t}, v\right)_2 = (-\text{curl}\ \mathbf{E}, v)_2 \tag{51a}$$

$$\left(\varepsilon_0 \varepsilon_\infty \frac{\partial \mathbf{E}}{\partial t}, \mathbf{u}\right)_2 = (\mathbf{curl}\, H, \mathbf{u})_2 - (\mathbf{J}, \mathbf{u})_2 \tag{51b}$$

$$\left(\frac{\partial \mathcal{P}}{\partial t}, \mathbf{w_1}\right)_F = (\mathcal{J}, \mathbf{w_1})_F \tag{51c}$$

$$\left(\frac{\partial \mathcal{J}}{\partial t}, \mathbf{w_2}\right)_F = (-2\nu\mathcal{J}, \mathbf{w_2})_F + \left(-\omega_0^2 \mathcal{P}, \mathbf{w_2}\right)_F + \left(\varepsilon_0 \omega_p^2 \mathbf{E}, \mathbf{w_2}\right)_F. \tag{51d}$$

We now have all the tools to prove stability for the 2D random Lorentz model.

Theorem 8.1. *Let $\mathcal{D} \subset \mathbb{R}^2$ and suppose that $\mathbf{E} \in C(0,T;H_0(\text{curl},\mathcal{D})) \cap C^1(0,T;(L^2(\mathcal{D}))^2)$, $\mathbf{P} \in C^1(0,T;\left(L^2(\mathcal{D})\right)^2)$, and $H(t) \in C^1(0,T;L^2(\mathcal{D}))$ are solutions of the weak formulation* (51) *for the Maxwell-Lorentz system* (47) *along with PEC boundary conditions. Then the system exhibits energy decay*

$$\mathcal{E}(t) \leq \mathcal{E}(0) \ \ \forall t \geq 0, \tag{52}$$

where the energy $\mathcal{E}(t)$ is defined as

$$\mathcal{E}(t) = \left(\left\| \sqrt{\mu_0}\, H(t) \right\|_2^2 + \left\| \sqrt{\varepsilon_0 \varepsilon_\infty}\, \mathbf{E}(t) \right\|_2^2 + \left\| \frac{\omega_0}{\omega_p \sqrt{\varepsilon_0}}\, \mathcal{P}(t) \right\|_F^2 + \left\| \frac{1}{\omega_p \sqrt{\varepsilon_0}}\, \mathcal{J}(t) \right\|_F^2 \right)^{\frac{1}{2}}. \tag{53}$$

Proof. We choose $v = H$, $\mathbf{u} = \mathbf{E}$, $\mathbf{w_1} = \mathcal{P}$, and $\mathbf{w_2} = \mathcal{J}$ in (51), multiply (51c) by $\frac{\omega_0^2}{\varepsilon_0 \omega_p^2}$, and multiply (51d) by $\frac{1}{\varepsilon_0 \omega_p^2}$. Then add all four equations together, utilizing our definition of energy and Green's formula.

$$\begin{aligned}
\frac{1}{2}\frac{d\mathcal{E}^2(t)}{dt} &= -\left(\text{curl}\ \mathbf{E}, H\right)_2 + \left(H, \text{curl}\ \mathbf{E}\right)_2 - \left(\mathbf{J}, \mathbf{E}\right)_2 + \left(\frac{\omega_0^2}{\varepsilon_0 \omega_p^2}\mathcal{J}, \mathcal{P}\right)_F \\
&\quad + \left(\frac{-2\nu}{\varepsilon_0 \omega_p^2}\mathcal{J}, \mathcal{J}\right)_F + \left(\frac{-\omega_0^2}{\varepsilon_0 \omega_p^2}\mathcal{P}, \mathcal{J}\right)_F + (\mathbf{E}, \mathcal{J})_F \\
&= -\left\| \sqrt{\frac{2\nu}{\varepsilon_0 \omega_p^2}}\, \mathcal{J} \right\|_F^2
\end{aligned}$$

After massive cancellation, we are left with

$$\frac{d\mathcal{E}^2(t)}{dt} = -2\left\| \sqrt{\frac{2\nu}{\varepsilon_0 \omega_p^2}} \mathcal{J} \right\|_F^2. \tag{54}$$

Rearranging, we get

$$\frac{d\mathcal{E}(t)}{dt} = \frac{-1}{\mathcal{E}(t)} \left\| \sqrt{\frac{2\nu}{\varepsilon_0 \omega_p^2}} \mathcal{J} \right\|_F^2 \leq 0. \tag{55}$$

Therefore the energy, $\mathcal{E}(t)$, is decreasing and $\mathcal{E}(t) \leq \mathcal{E}(0)\ \forall t > 0$. □

8.2. **Maxwell-PC Lorentz-FDTD.**

8.2.1. *Discretization.* For our discrete approximation to converge to the true solution, it must be consistent and stable. Consistency is guaranteed by FDTD. To show the stability of the Lorentz-FDTD model in two dimensions, we borrow notation from [7] that will ease the proof. First, consider the space $(x,y) \in [0,a] \times [0,b]$ for $t \in [0,T]$. Choose integers L, J, and N to discretize the space so that $\Delta x = a/L,\ \Delta y = b/J,$ and $\Delta t = T/N$. Let $x_\ell = \ell \Delta x,\ y_j = j\Delta y,$ and $t^n = n\Delta t$. We stagger three discrete meshes in the x and y directions, and two discrete meshes in the time domain:

$$\tau_h^{E_x} := \left\{ \left(x_{\ell+\frac{1}{2}}, y_j \right) | 0 \leq \ell \leq L-1, 0 \leq j \leq J \right\} \tag{56}$$

$$\tau_h^{E_y} := \left\{ \left(x_\ell, y_{j+\frac{1}{2}} \right) | 0 \leq \ell \leq L, 0 \leq j \leq J-1 \right\} \tag{57}$$

$$\tau_h^{H} := \left\{ \left(x_{\ell+\frac{1}{2}}, y_{j+\frac{1}{2}} \right) | 0 \leq \ell \leq L-1, 0 \leq j \leq J-1 \right\} \tag{58}$$

$$\tau_t^{E} := \{ (t^n) | 0 \leq n \leq N \} \tag{59}$$

$$\tau_t^{H} := \left\{ \left(t^{n+\frac{1}{2}} \right) | 0 \leq n \leq N-1 \right\}. \tag{60}$$

The field variables are discretized as follows:

$$E_x, P_x \in \tau_h^{E_x}, \quad E_y, P_y \in \tau_h^{E_y}, \quad H \in \tau_h^H, \quad E_x, E_y, P_x, P_y \in \tau_t^E, \quad H \in \tau_t^H.$$

Let x_α, y_β be a node on any spatial mesh, and t^γ a node on either temporal mesh. If U is a field variable, we define the grid functions as

$$U_{\alpha,\beta}^\gamma \approx U(x_\alpha, y_\beta, t^\gamma).$$

We define the time difference operator and time averaging operator as

$$\delta_t U_{\alpha,\beta}^\gamma := \frac{U_{\alpha,\beta}^{\gamma+\frac{1}{2}} - U_{\alpha,\beta}^{\gamma-\frac{1}{2}}}{\Delta t} \tag{61}$$

$$\overline{U}_{\alpha,\beta}^\gamma := \frac{U_{\alpha,\beta}^{\gamma+\frac{1}{2}} + U_{\alpha,\beta}^{\gamma-\frac{1}{2}}}{2} \tag{62}$$

and the spatial difference operators in the x and y direction as

$$\delta_x U^{\gamma}_{\alpha,\beta} := \frac{U^{\gamma}_{\alpha+\frac{1}{2},\beta} - U^{\gamma}_{\alpha-\frac{1}{2},\beta}}{\Delta x} \tag{63}$$

$$\delta_y U^{\gamma}_{\alpha,\beta} := \frac{U^{\gamma}_{\alpha,\beta+\frac{1}{2}} - U^{\gamma}_{\alpha,\beta-\frac{1}{2}}}{\Delta y}. \tag{64}$$

Next, we define the L^2 normed spaces

$$\mathbb{V}_E := \left\{ \mathbf{F} : \tau_h^{E_x} \times \tau_h^{E_y} \longrightarrow \mathbb{R}^2 \mid \mathbf{F} = (F_{x_{l+\frac{1}{2},j}}, F_{y_{l,j+\frac{1}{2}}})^T, \|\mathbf{F}\|_E < \infty \right\} \tag{65}$$

$$\mathbb{V}_H := \left\{ U : \tau_h^{H} \longrightarrow \mathbb{R} \mid U = (U_{l+\frac{1}{2},j+\frac{1}{2}}), \|U\|_H < \infty \right\} \tag{66}$$

with the following discrete norms and inner products

$$\|\mathbf{F}\|_E^2 = \Delta x \Delta y \sum_{\ell=0}^{L-1} \sum_{j=0}^{J-1} \left(|F_{x_{\ell+\frac{1}{2},j}}|^2 + |F_{y_{\ell,j+\frac{1}{2}}}|^2 \right), \forall\, \mathbf{F} \in \mathbb{V}_E \tag{67}$$

$$(\mathbf{F},\mathbf{G})_E = \Delta x \Delta y \sum_{\ell=0}^{L-1} \sum_{j=0}^{J-1} \left(F_{x_{\ell+\frac{1}{2},j}} G_{x_{\ell+\frac{1}{2},j}} + F_{y_{\ell,j+\frac{1}{2}}} G_{y_{\ell,j+\frac{1}{2}}} \right), \forall\, \mathbf{F},\mathbf{G} \in \mathbb{V}_E \tag{68}$$

$$\|U\|_H^2 = \Delta x \Delta y \sum_{\ell=0}^{L-1} \sum_{j=0}^{J-1} |U_{\ell+\frac{1}{2},j+\frac{1}{2}}|^2, \forall\, U \in \mathbb{V}_H \tag{69}$$

$$(U,V)_H = \Delta x \Delta y \sum_{\ell=0}^{L-1} \sum_{j=0}^{J-1} U_{\ell+\frac{1}{2},j+\frac{1}{2}} V_{\ell+\frac{1}{2},j+\frac{1}{2}}, \forall\, U,V \in \mathbb{V}_H. \tag{70}$$

Finally, we define discrete curl operators on the staggered L^2 normed spaces as

$$\begin{aligned} &\mathrm{curl}_h : \mathbb{V}_E \longrightarrow \mathbb{V}_H && \mathbf{curl}_h : \mathbb{V}_H \longrightarrow \mathbb{V}_E \\ &\mathrm{curl}_h \mathbf{F} := \delta_x F_y - \delta_y F_x && \mathbf{curl}_h U := (\delta_y U, -\delta_x U)^T. \end{aligned} \tag{71}$$

We require that PEC conditions hold for all $\mathbf{F} \in \mathbb{V}_E$ so that

$$F_{x_{\ell+\frac{1}{2},0}} = F_{x_{\ell+\frac{1}{2},J}} = 0, \qquad 0 \le \ell \le L \tag{72}$$

$$F_{y_{0,j+\frac{1}{2}}} = F_{x_{L,j+\frac{1}{2}}} = 0, \qquad 0 \le j \le J. \tag{73}$$

Then discrete integration by parts shows that Green's curl identity holds for our discrete system as well:

$$(\mathrm{curl}_h \mathbf{E}, H)_H = (\mathbf{E}, \mathbf{curl}_h H)_E. \tag{74}$$

The definitions are tedious, but we see that all discrete operators, spaces, and inner products are closely related to the continuous case, as discussed in the previous section.

8.2.2. *2D Yee Scheme.* Utilizing the operators defined in (61)–(64), we can write out the discrete forms of (47):

$$\delta_t H^n_{\ell+\frac{1}{2},j+\frac{1}{2}} = \frac{1}{\mu_0}\left(\delta_y E^n_{x_{\ell+\frac{1}{2},j+\frac{1}{2}}} - \delta_x E^n_{y_{\ell+\frac{1}{2},j+\frac{1}{2}}}\right) \tag{75a}$$

$$\varepsilon_0\varepsilon_\infty\delta_t E^{n+\frac{1}{2}}_{x_{\ell+\frac{1}{2},j}} = \delta_y H^{n+\frac{1}{2}}_{\ell+\frac{1}{2},j} - \overline{\vec{\beta}}^{n+\frac{1}{2}}_{0,x_{\ell+\frac{1}{2},j}} \tag{75b}$$

$$\varepsilon_0\varepsilon_\infty\delta_t E^{n+\frac{1}{2}}_{y_{\ell,j+\frac{1}{2}}} = -\delta_x H^{n+\frac{1}{2}}_{\ell,j+\frac{1}{2}} - \overline{\vec{\beta}}^{n+\frac{1}{2}}_{0,y_{\ell,j+\frac{1}{2}}} \tag{75c}$$

$$\delta_t \vec{\alpha}^{n+\frac{1}{2}}_{x_{\ell+\frac{1}{2},j}} = \overline{\vec{\beta}}^{\,n+\frac{1}{2}}_{x_{\ell+\frac{1}{2},j}} \tag{75d}$$

$$\delta_t \vec{\alpha}^{n+\frac{1}{2}}_{y_{\ell,j+\frac{1}{2}}} = \overline{\vec{\beta}}^{\,n+\frac{1}{2}}_{y_{\ell,j+\frac{1}{2}}} \tag{75e}$$

$$\delta_t \vec{\beta}^{\,n+\frac{1}{2}}_{x_{\ell+\frac{1}{2},j}} = -\omega_0^2\overline{\vec{\alpha}}^{n+\frac{1}{2}}_{x_{\ell+\frac{1}{2},j}} - 2\nu\overline{\vec{\beta}}^{n+\frac{1}{2}}_{x_{\ell+\frac{1}{2},j}} + \hat{e}_1\varepsilon_0\omega_p^2\overline{E}^{n+\frac{1}{2}}_{x_{\ell+\frac{1}{2},j}} \tag{75f}$$

$$\delta_t \vec{\beta}^{\,n+\frac{1}{2}}_{y_{\ell,j+\frac{1}{2}}} = -\omega_0^2\overline{\vec{\alpha}}^{n+\frac{1}{2}}_{y_{\ell,j+\frac{1}{2}}} - 2\nu\overline{\vec{\beta}}^{n+\frac{1}{2}}_{y_{\ell,j+\frac{1}{2}}} + \hat{e}_1\varepsilon_0\omega_p^2\overline{E}^{n+\frac{1}{2}}_{y_{\ell,j+\frac{1}{2}}}. \tag{75g}$$

However, we can simplify the work by writing the equations in vector notation, where we recall that $\mathbf{F} \in \mathbb{V}_E$ are defined on $\tau_h^{E_x} \times \tau_h^{E_y}$ and $U \in \mathbb{V}_H$ are defined on τ_h^H:

$$\delta_t H^n + \frac{1}{\mu_0}\left(\mathrm{curl}_h \mathbf{E}^n\right) = 0 \tag{76a}$$

$$\varepsilon_0\varepsilon_\infty\delta_t \mathbf{E}^{n+\frac{1}{2}} = \left(\mathbf{curl}_h H^{n+\frac{1}{2}}\right) - \hat{e}_1^T\overline{\vec{\beta}}^{n+\frac{1}{2}} \tag{76b}$$

$$\delta_t \vec{\alpha}^{n+\frac{1}{2}} = \overline{\vec{\beta}}^{\,n+\frac{1}{2}} \tag{76c}$$

$$\delta_t \vec{\beta}^{n+\frac{1}{2}} = -\omega_0^2\overline{\vec{\alpha}}^{\,n+\frac{1}{2}} - 2\nu\overline{\vec{\beta}}^{\,n+\frac{1}{2}} + \hat{e}_1\varepsilon_0\omega_p^2\overline{\mathbf{E}}^{n+\frac{1}{2}}. \tag{76d}$$

We must also define another space and inner product for the random polarization in vector notation as $\vec{\alpha}$ and $\vec{\beta}$ are now $2 \times p$ matrices:

$$\mathbb{V}_\alpha := \left\{\vec{\alpha} : \tau_h^{E_x} \times \tau_h^{E_y} \longrightarrow \mathbb{R}^2 \times \mathbb{R}^p \;\middle|\; \vec{\alpha} = [\alpha_0, \ldots, \alpha_{p-1}], \alpha_k \in \mathbb{V}_E, \|\vec{\alpha}\|_\alpha < \infty\right\}$$

where the discrete L^2 grid norm and inner product are defined as

$$\|\vec{\alpha}\|_\alpha^2 = \sum_{k=0}^{p-1} \|\alpha_k\|_E^2, \quad \forall\, \vec{\alpha} \in \mathbb{V}_\alpha$$

$$(\vec{\alpha}, \vec{\beta})_\alpha = \sum_{k=0}^{p-1} \left(\alpha_k, \beta_k\right)_E, \quad \forall\, \vec{\alpha}, \vec{\beta} \in \mathbb{V}_\alpha.$$

8.2.3. *Energy Decay and Stability.* We choose both spacial steps to be equal ($\Delta x = \Delta y = h$), and require that the usual CFL condition for two dimensions holds:

$$\sqrt{2}c_\infty \Delta t \leq h. \tag{77}$$

Theorem 8.2 (Energy Decay for Maxwell-PC Lorentz-FDTD)**.** *If the stability condition* (77) *is satisfied, then the Yee scheme for the 2D TE mode Maxwell-PC Lorentz system given in* (75) *satisfies the discrete identity*

$$\delta_t \mathcal{E}_h^{n+\frac{1}{2}} = \frac{-1}{\overline{\mathcal{E}}_h^{n+\frac{1}{2}}} \left\| \sqrt{\frac{2\nu}{\varepsilon_0 \omega_p^2}} \overline{\vec{\beta}}_h^{n+\frac{1}{2}} \right\|_\alpha^2 \tag{78}$$

for all n where

$$\mathcal{E}_h^n = \left(\mu_0 (H^{n+\frac{1}{2}}, H^{n-\frac{1}{2}})_H + \left\| \sqrt{\varepsilon_0 \varepsilon_\infty}\, \mathbf{E}^n \right\|_E^2 + \left\| \sqrt{\frac{\omega_0^2}{\varepsilon_0 \omega_p^2}} \vec{\alpha}^n \right\|_\alpha^2 + \left\| \sqrt{\frac{1}{\varepsilon_0 \omega_p^2}} \vec{\beta}^n \right\|_\alpha^2 \right)^{1/2} \tag{79}$$

defines a discrete energy.

Proof. Multiplying both sides of (76b) by $\Delta x \Delta y \overline{\mathbf{E}}^{n+\frac{1}{2}}$ and summing over all nodes on $\tau_h^{E_x} \times \tau_h^{E_y}$, we obtain

$$\varepsilon_0 \varepsilon_\infty (\delta_t \mathbf{E}^{n+\frac{1}{2}}, \overline{\mathbf{E}}^{n+\frac{1}{2}})_E = (\mathbf{curl}_h H^{n+\frac{1}{2}}, \overline{\mathbf{E}}^{n+\frac{1}{2}})_E - (\hat{e}_1^T \overline{\vec{\beta}}^{n+\frac{1}{2}}, \overline{\mathbf{E}}^{n+\frac{1}{2}})_E \tag{80}$$

which is equivalent to

$$\frac{\varepsilon_0 \varepsilon_\infty}{2\Delta t} \left[\|\mathbf{E}^{n+1}\|_E^2 - \|\mathbf{E}^n\|_E^2 \right] = (\mathbf{curl}_h H^{n+\frac{1}{2}}, \overline{\mathbf{E}}^{n+\frac{1}{2}})_E - (\hat{e}_1^T \overline{\vec{\beta}}^{n+\frac{1}{2}}, \overline{\mathbf{E}}^{n+\frac{1}{2}})_E. \tag{81}$$

Next, we take the average of (76a) at n and $n+1$, multiply by $\Delta x \Delta y H^{n+\frac{1}{2}}$, and sum over τ_h^H to get

$$\mu_0 (\delta_t \overline{H}^{n+\frac{1}{2}}, H^{n+\frac{1}{2}})_H + (\mathrm{curl}_h \overline{\mathbf{E}}^{n+\frac{1}{2}}, H^{n+\frac{1}{2}})_H = 0 \tag{82}$$

which is equivalent to

$$\frac{\mu_0}{2\Delta t} \left[(H^{n+\frac{3}{2}}, H^{n+\frac{1}{2}})_H - (H^{n+\frac{1}{2}}, H^{n-\frac{1}{2}})_H \right] + (\mathrm{curl}_h \overline{\mathbf{E}}^{n+\frac{1}{2}}, H^{n+\frac{1}{2}})_H = 0. \tag{83}$$

Multiplying (76c) by $\Delta x \Delta y \overline{\vec{\alpha}}^{n+\frac{1}{2}}$ and summing over $\tau_h^{E_x} \times \tau_h^{E_y}$, we get

$$\left(\delta_t \vec{\alpha}^{n+\frac{1}{2}}, \overline{\vec{\alpha}}^{\,n+\frac{1}{2}} \right)_\alpha = \left(\overline{\vec{\beta}}^{n+\frac{1}{2}}, \overline{\vec{\alpha}}^{\,n+\frac{1}{2}} \right)_\alpha. \tag{84}$$

We multiply by $\frac{\omega_0^2}{\varepsilon_0 \omega_p^2}$ and rewrite as

$$\frac{\omega_0^2}{2\Delta t \varepsilon_0 \omega_p^2} \left[\|\vec{\alpha}^{n+1}\|_\alpha^2 - \|\vec{\alpha}^n\|_\alpha^2 \right] = \frac{\omega_0^2}{\varepsilon_0 \omega_p^2} \left(\overline{\vec{\beta}}^{n+\frac{1}{2}}, \overline{\vec{\alpha}}^{\,n+\frac{1}{2}} \right)_\alpha. \tag{85}$$

Lastly, we multiply (76d) by $\Delta x\Delta y\vec{\overline{\beta}}^{n+\frac{1}{2}}$ and sum over $\tau_h^{E_x}\times\tau_h^{E_y}$ to obtain

(86)
$$\left(\delta_t\vec{\beta}^{n+\frac{1}{2}},\vec{\overline{\beta}}^{\,n+\frac{1}{2}}\right)_\alpha=-\omega_0^2\left(\vec{\overline{\alpha}}^{n+\frac{1}{2}},\vec{\overline{\beta}}^{\,n+\frac{1}{2}}\right)_\alpha-2\nu\left(\vec{\overline{\beta}}^{n+\frac{1}{2}},\vec{\overline{\beta}}^{\,n+\frac{1}{2}}\right)_\alpha+\left(\hat{e}_1\varepsilon_0\omega_p^2\overline{\mathbf{E}}^{n+\frac{1}{2}},\vec{\overline{\beta}}^{\,n+\frac{1}{2}}\right)_\alpha.$$

We multiply by $\frac{1}{\varepsilon_0\omega_p^2}$ and rewrite as

(87)
$$\frac{1}{2\Delta t\varepsilon_0\omega_p^2}\left[\|\vec{\beta}^{n+1}\|_\alpha^2-\|\vec{\beta}^{n}\|_\alpha^2\right]=\frac{-\omega_0^2}{\varepsilon_0\omega_p^2}\left(\vec{\overline{\alpha}}^{n+\frac{1}{2}},\vec{\overline{\beta}}^{\,n+\frac{1}{2}}\right)_\alpha-\frac{2\nu}{\varepsilon_0\omega_p^2}\left(\vec{\overline{\beta}}^{n+\frac{1}{2}},\vec{\overline{\beta}}^{\,n+\frac{1}{2}}\right)_\alpha+\left(\hat{e}_1\overline{\mathbf{E}}^{n+\frac{1}{2}},\vec{\overline{\beta}}^{\,n+\frac{1}{2}}\right)_\alpha.$$

Adding (81), (83), (85), and (87), then using the definition (79), we have

$$\frac{1}{2\Delta t}\left\{(\mathcal{E}_h^{n+1})^2-(\mathcal{E}_h^n)^2\right\}=-\frac{2\nu}{\varepsilon_0\omega_p^2}\left(\vec{\overline{\beta}}^{n+\frac{1}{2}},\vec{\overline{\beta}}^{\,n+\frac{1}{2}}\right)_\alpha \tag{88}$$

where we noticed that

$$(\hat{e}_1\overline{\mathbf{E}}^{n+\frac{1}{2}},\vec{\overline{\beta}}^{\,n+\frac{1}{2}})_\alpha=(\hat{e}_1^T\vec{\overline{\beta}}^{n+\frac{1}{2}},\overline{\mathbf{E}}^{n+\frac{1}{2}})_E.$$

We can rewrite (88) in the form

$$\frac{\mathcal{E}_h^{n+1}-\mathcal{E}_h^n}{\Delta t}=-\left(\frac{2}{\mathcal{E}_h^{n+1}+\mathcal{E}_h^n}\right)\left\|\sqrt{\frac{2\nu}{\varepsilon_0\omega_p^2}}\vec{\overline{\beta}}^{n+\frac{1}{2}}\right\|_\alpha^2. \tag{89}$$

We prove that (79) is a discrete energy (or positive definite function) by rewriting as

$$(\mathcal{E}_h^n)^2=\mu_0\|\overline{H}^n\|_H^2+\varepsilon_0\varepsilon_\infty(\mathbf{E}^n,\mathcal{A}_h\mathbf{E}^n)_E+\frac{1}{\varepsilon_0\omega_p^2}\left(\omega_0\vec{\overline{\alpha}}^{n},\omega_0\vec{\overline{\alpha}}^{n}\right)_\alpha+\frac{2\nu}{\varepsilon_0\omega_p^2}\left(\vec{\overline{\beta}}_h^{n+\frac{1}{2}},\vec{\overline{\beta}}_h^{n+\frac{1}{2}}\right)_\alpha \tag{90}$$

where $\mathcal{A}_h$ is positive definite when the CFL condition is satisfied. The work follows exactly as in [7]. □

9. Conclusion and Future Work

We showed in the frequency domain that applying a distribution to ω_0^2 can produce significantly better fits than the deterministic Lorentz model. Then, we used Polynomial Chaos and finite differences with the first order Yee Scheme to discretize our system in the time domain. Through simulations it was shown that the Polynomial Chaos method converged quickly for the number of polynomials used in the expansion. For the inverse problem, we compared a single frequency interrogating signal with a UWB pulse. The distributed model only fit better than the deterministic model over a range of frequencies as implied by the complex permittivity plots in the frequency domain. Finally, we showed stability of the random Lorentz model and convergence of the discretization.

There were several areas of this work that could be explored further. Even though we laid the mathematical groundwork for the beta distribution, we focused primarily on uniform distributions in our simulations. The simulations and results could be extended fully to beta distributions. Since the high frequencies of the Lorentz model require very small time steps, we would like to increase

the duration of the simulations to see if it provides better differentiation between models. We also mentioned the importance of accurately estimating the true parameters of a material from noisy data. We would need to run many simulations to gather statistical data in order to make any significant conclusions.

REFERENCES

[1] 6.007 electromagnetic energy: From motors to laser, Spring 2011. License: Creative Commons BY-NC-SA.

[2] H Thomas Banks, Michael W Buksas, and Tao Lin. *Electromagnetic Material Interrogation Using Conductive Interfaces and Acoustic Wavefronts*. SIAM, 2000.

[3] H Thomas Banks and Karl Kunisch. *Estimation Techniques for Distributed Parameter Systems*. Springer Science & Business Media, 1989.

[4] Harvey Thomas Banks, Jared Catenacci, and Shuhua Hu. Method comparison for estimation of distributed parameters in permittivity models using reflectance. *Eurasian Journal of Mathematical and Computer Applications*, 3(2):4–24, 2015.

[5] HT Banks and NL Gibson. Electromagnetic inverse problems involving distributions of dielectric mechanisms and parameters. *Quarterly of Applied Mathematics*, 64(4):749, 2006.

[6] E. Bela and E. Hortsch. Generalized polynomial chaos and dispersive dielectric media. In N. L. Gibson, editor, *REU Program at Oregon State University Proceedings*, 2010.

[7] V.A. Bokil and N.L. Gibson. Convergence analysis of yee schemes for maxwell's equations in debye and lorentz dispersive media. *International Journal of Numerical Analysis & Modeling*, 11(4), 2014.

[8] Daniel E Finkel. Direct optimization algorithm user guide. *Center for Research in Scientific Computation, North Carolina State University*, 2, 2003.

[9] Brian McKenzie. Polynomial chaos expansions for random ordinary differential equations. Technical report, Oregon State University, http://hdl.handle.net/1957/38475, 2012.

[10] Kurt E Oughstun and Natalie A Cartwright. On the lorentz-lorenz formula and the lorentz model of dielectric dispersion. *Optics express*, 11(13):1541–1546, 2003.

[11] Marvin R. Querry, Richard C. Waring, Wayne E. Holland, G. Michael Hale, and William Nijm. Optical constants in the infrared for aqueous solutions of nacl. *J. Opt. Soc. Am.*, 62(7):849–855, Jul 1972.

[12] Dongbin Xiu. *Numerical Methods for Stochastic Computations: A Spectral Method Approach*. Princeton university press, 2010.

[13] Kane Yee. Numerical solution of initial boundary value problems involving maxwell's equations in isotropic media. *IEEE Transactions on antennas and propagation*, 14(3):302–307, 1966.

CALIFORNIA STATE POLYTECHNIC UNIVERSITY, POMONA
E-mail address: jacquelinea1@cpp.edu

WALLA WALLA UNIVERSITY
E-mail address: andrew.fisher@wallawalla.edu